AGU PUBLICATIONS

JGR

Journal of Geophysical Research: Space Physics

RESEARCH ARTICLE
10.1002/2016JA022436

Key Points:
- Enhanced and depressed flux tubes are the same magnetic flux returning from the tail reconnection
- The cross sections of the flux tubes are close to circular
- Magnetic flux and plasma transportation rate calculated based on tail reconnection are reasonable

Supporting Information:
- Supporting Information S1
- Table S1
- Table S2

Correspondence to:
H. R. Lai,
hlai@igpp.ucla.edu

Citation:
Lai, H. R., C. T. Russell, Y. D. Jia, H. Y. Wei, and M. K. Dougherty (2016), Transport of magnetic flux and mass in Saturn's inner magnetosphere, *J. Geophys. Res. Space Physics*, *121*, 3050–3057, doi:10.1002/2016JA022436.

Received 25 JAN 2016
Accepted 15 MAR 2016
Accepted article online 21 MAR 2016
Published online 9 APR 2016

Transport of magnetic flux and mass in Saturn's inner magnetosphere

H. R. Lai[1], C. T. Russell[1], Y. D. Jia[1], H. Y. Wei[1], and M. K. Dougherty[2]

[1]EPSS and IGPP, UCLA, Los Angeles, California, USA, [2]Department of Physics, Imperial College London, London, UK

Abstract It is well accepted that cold plasma sourced by Enceladus is ultimately lost to the solar wind, while the magnetic flux convecting outward with the plasma must return to the inner magnetosphere. However, whether the interchange or reconnection, or a combination of the two processes is the dominant mechanism in returning the magnetic flux is still under debate. Initial Cassini observations have shown that the magnetic flux returns in the form of flux tubes in the inner magnetosphere. Here we investigate those events with 10 year Cassini magnetometer data and confirm that their magnetic signatures are determined by the background plasma environments: inside (outside) the plasma disk, the returning magnetic field is enhanced (depressed) in strength. The distribution, temporal variation, shape, and transportation rate of the flux tubes are also characterized. The flux tubes break into smaller ones as they convect in. The shape of their cross section is closer to circular than fingerlike as produced in the simulations based on the interchange mechanism. In addition, no sudden changes in any flux tube properties can be found at the "boundary" which has been claimed to separate the reconnection and interchange-dominant regions. On the other hand, reasonable cold plasma loss rate and outflow velocity can be obtained if the transport rate of the magnetic flux matches the reconnection rate, which supports reconnection alone as the dominant mechanism in unloading the cold plasma from the inner magnetosphere and returning the magnetic flux from the tail.

1. Introduction

The rapidly rotating planets, Saturn and Jupiter, both with plasma sources internal to their magnetosphere, have many similarities in their magnetospheric dynamics. At Saturn, water-group neutrals are ionized after being released from the plume of Enceladus at 4 R_S, forming a plasma source of typical strength 12–250 kg/s [*Bagenal and Delamere*, 2011, and references therein]. This plasma is then accelerated to subcorotation by its magnetic connection to the ionosphere, convects outward, and is shed to the solar wind ultimately. In this plasma transfer process, the magnetic flux also convects outward. To conserve the total magnetic flux imposed on the magnetosphere by the planet's internal dynamo, the outward-convected magnetic flux has to return to the inner magnetosphere at exactly the same average rate.

At Jupiter, the magnetic flux returns in the form of flux tubes, characterized by intermittent short duration increases in the magnetic field strength with abrupt onset and recovery in Io's plasma torus [*Russell et al.*, 2000, 2001]. Similar flux tubes were detected from the magnetic field data obtained during the very first orbits of Cassini at Saturn [*Andre et al.*, 2005]. This time, they consisted of both enhancements and depressions in the field strength, which are referred to as enhanced flux tubes and depressed flux tubes, respectively. Although the magnetic signatures are opposite, the plasma in both types of flux tubes has the same properties: a significant density drop in the low-energy plasma population and an increase in plasma temperature due to the appearance of a hotter plasma population [*Andre et al.*, 2007]. In their study, even with a sparse data set, the latitudinal dependence of the opposite magnetic signature is evident, i.e., enhanced flux tubes are detected near the equator, while depressed ones are detected off the equator. The investigation of energy dispersion of the hot plasma contained in the depressed flux tubes found that the ages of most flux tubes are less than 10.8 h (Saturn's rotation period) [*Hill et al.*, 2005; *Chen and Hill*, 2008].

The identical plasma properties inside both types of flux tubes suggest that they are different segments of the same flux tube from the same origin. The apparent opposite magnetic field signatures are due to the different background plasma environments that these flux tubes are sitting in. Figure 1 sketches the two situations when Cassini encounters a flux tube, where the two opposite types of magnetic perturbations are detected.

Enceladus sources water-group gas and plasma into a plasma disk from 2.5 to 8 R_S (Saturn radius) around Saturn. The density of the plasma peaks at the equator and decreases exponentially off the equator, dropping

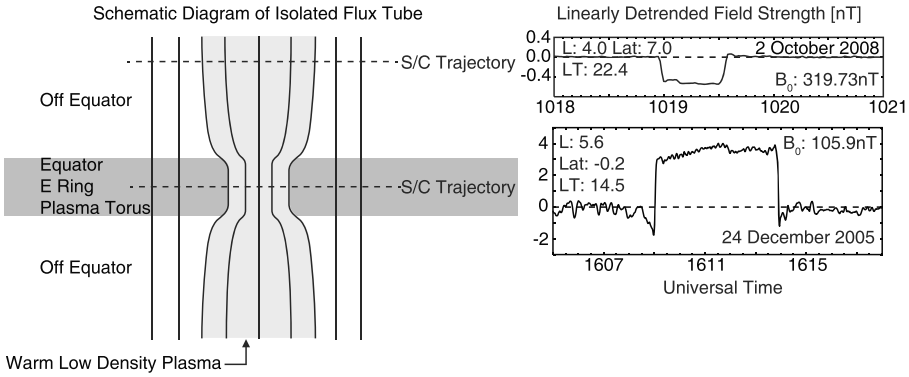

Figure 1. (left) A cartoon illustrating the different magnetic signatures in different segments of the same flux tube. To balance the total pressure across the boundaries, the low-density but high-temperature flux tube is compressed in the plasma torus and expands off the equator. (right) Examples of enhanced and depressed flux tubes. Their *L* value, latitude (Lat), local time (LT), and background field strength (B_0) is listed at the corner. Note the different vertical scales of the field strength between the enhanced and depressed flux tubes.

by orders of magnitude beyond 2 R_S from the equator due to the centripetal force [*Holmberg et al*., 2012]. As the flux tubes contain ions with a temperature of several keV, it takes barely a few minutes for the transverse pressure to reach balance across a flux tube, which is typically less than 1 R_S in azimuthal direction [*Hill et al*., 2005]. As shown in Figure 1, the segment of flux tubes inside the plasma disk is compressed by surrounding cold and dense plasma, showing an enhancement in the field strength, while the part of the flux tube outside the plasma disk expands into the surrounding cold and tenuous plasma, resulting in decreased field strength. Such pressure balance also applies to the enhanced flux tubes detected in Io's torus. We note that the magnitudes of compression and expansion in Figure 1 are exaggerated. As listed in the flux tube examples, the field strength enhancement or depression is at most several nanotesla, less than a few percent in a hundred or more nanotesla background field.

Even after 10 years of Cassini observations, it is still not clear how the magnetic field sheds the cold plasma population and returns to the inner magnetosphere. Several mechanisms have been suggested. The first one is interchange hypothesis. *Siscoe and Summers* [1981] calculated the Saturnian magnetosphere to be centrifugally unstable outside the plasma torus, independent of local time. Therefore, interchange between inner mass-loaded magnetic field lines and outer magnetic field lines carrying relatively tenuous but hot plasma can happen everywhere in the plasma disk. This interchange-driven instability has been modeled using the Rice Convection Model [*Wu*, 2009] and later with magnetohydrodynamic modeling [*Winglee et al*., 2013]. In both simulations, the magnetic flux and plasma convect inward and outward in the form of finger-shaped structures rooted in the plasma disk. The second mechanism is the reconnection hypothesis, which has been developed first in the Jovian magnetosphere [*Russell et al*., 2000]: tail reconnection, known as the Vasyliunas cycle [*Vasyliunas*, 1983], sheds the mass to form plasma-depleted flux tubes. These flux tubes then convect to the inner magnetosphere buoyantly and at the same time corotate with the magnetosphere. This hypothesis explains the depleted ion composition correlated with the field perturbations and is consistent with our Figure 1 illustration. This model suggests that the fast flow shooting back from the reconnection X line breaks into flux tubes, which appear as bubbles if sliced in the equatorial plane. *Thomsen et al*. [2015] combined the two hypotheses into a third hypothesis: tail reconnection creates plasma-depleted flux tubes; they then convect to the inner magnetosphere and stop at $L \sim 8.6$, where the cold and dense plasma holds off the hot and tenuous plasma from the tail; interchange then takes place within $L \sim 8.6$, injects the hot plasma, and lets the cold plasma flow out. The third hypothesis believes that the hot plasma population seen in the flux tubes in the inner magnetosphere [*Hill et al*., 2005] is the same plasma at $L \sim 8.6$, instead of the plasma from the tail reconnection site.

In this paper, we test the magnetic flux and plasma circulation hypotheses with a set of enhanced and depressed flux tubes identified from 10 year Cassini magnetometer observations. The next section of this paper describes the data and selection criteria. Then we investigate the statistical properties of the flux tubes. This is followed by the study considering the shape and transportation rate of the magnetic flux. The final section concludes this study.

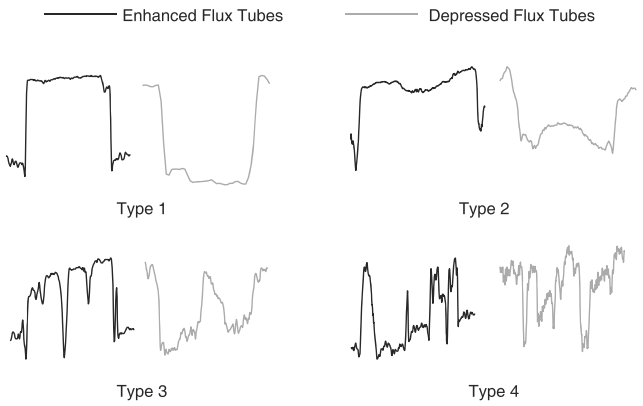

Figure 2. Four types of flux tubes identified from the magnetic field data classified by the absolute change in field strength.

2. Data Set and Selection Criteria

One second magnetic field data measured by the Cassini magnetometer [*Dougherty et al.*, 2004] for almost 10 years (from 27 February 2005 to 25 January 2015) are used to search for the flux tubes. During this period, Cassini has completed 209 revolutions around Saturn, covering a radial distance from inside 3 R_S to over 60 R_S and a latitudinal range from about $-75°$ to 75°. In earlier studies, Cassini data obtained within 10 R_S are investigated [*Andre et al.*, 2005, 2007; *Hill et al.*, 2005; *Chen and Hill*, 2008]. Since the birthplace of plasma-depleted flux tubes may be farther out, we extend the survey region to $L = 18$. Here a dipole model is employed to calculate the L from the event location, where $L = r/\cos^2\theta$. Here r is the radial distance and θ is the latitude. As the typical subsolar magnetopause distance at Saturn is about 22 R_S, this dipolar assumption is generally valid in our region of interest.

The KRTP (Kronocentric radial theta phi) coordinate system is used in this study: r is pointing radially away from the center of Saturn to the location of the spacecraft, ϕ is parallel to the kronographic equator and positive in the direction of corotation, and θ is southward, completing the right-handed set.

We search for candidate events by visually inspecting 6 h linearly detrended magnetic field data, and the following criteria are applied to collect unambiguous events: (1) the estimated L is less than 18, (2) the perturbations last over 30 s, (3) the abrupt increase or decrease relative to the background field strength is at least twice the background noise. Here "abrupt" means that the time for the rise/decrease in the magnetic field strength at the edges of the tubes is less than half the duration of the flux tube.

These events are further classified into four types by the absolute change in the field strength, as shown in Figure 2. Type 1 events are generally the ideal cases with sharp boundaries and step-like increase/decrease, where the field strength jumps to and persists in a relatively constant value. Type 2 events have crater-like structures in the middle, in addition to the step-like increase/decrease across the flux tube boundary. When the minimum perturbation of the "crater" temporarily returns the signal to the background value, these flux tubes are classified as type 3 events. A type 4 event is filled with jumps between maximum perturbation and zero perturbation and can be taken as a cluster of individual flux tubes. Since we have a statistically significant number of events in each of the first three categories and the type 4 events are believed to represent fragmental flux tubes near the end of their identifiable lives, if not specified, our statistical studies in this paper are based on the type 1, type 2 and type 3 events.

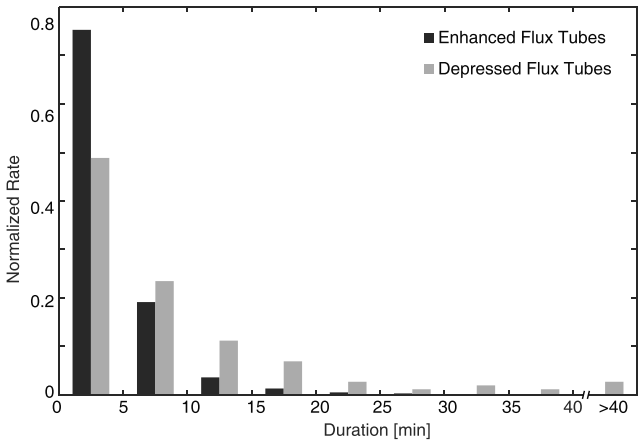

Figure 3. Duration distribution of the flux tubes. The vertical axis shows the number in each bin normalized by the total counts.

3. Statistical Properties

In total, 392 enhanced and 260 depressed flux tubes (type 4 events excluded) are identified from the magnetic field data. In our introduction, examples of typical flux tubes with detrended magnetic field profiles are given with detailed parameters in Figure 1. The duration of all the events is counted and compared in

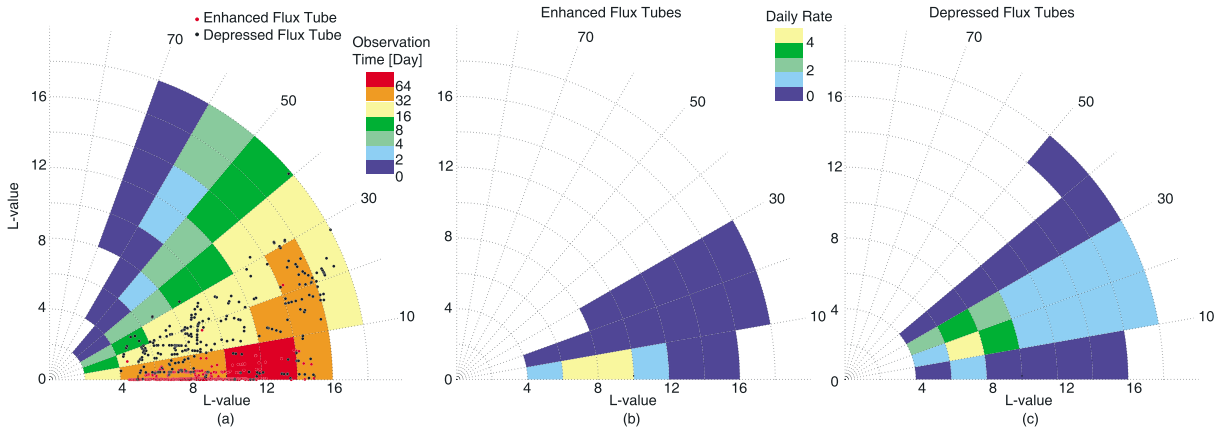

Figure 4. (a) Locations of the flux tubes represented by black (depressed) and red (enhanced) dots. The color shows accumulated observation time as a function of *L* and latitude. (b) Daily rate of the enhanced flux tubes. (c) Daily rate of the depressed flux tubes. The color coded accumulated observation time and the daily rates are overlapping results: when calculating these values in each pixel, the observation time and the counts of the flux tubes in its neighboring width (within a half pixel) are also counted.

Figure 3. It appears that flux tubes with durations of 5 min or less consist of over 75% of the enhanced flux tubes, and this percentage decreases to 49% for the depressed flux tubes; 8% of enhanced flux tubes last more than 20 min, while 2.7% of depressed flux tubes last longer than 40 min. Therefore, the depressed flux tubes last generally longer than the enhanced flux tubes. We note that in a bubble model, a short duration does not necessarily indicate a small flux tube. It is also possible that the spacecraft skimmed through only the flank of the flux tube. In contrast, in the finger model, the observed time directly reveals the width of the finger.

With a much larger database, we repeat Andre's study. Figure 4 shows the latitudinal and *L* distribution of the flux tubes. Here we assume that the distribution of the flux tubes is equatorial symmetric, so the northern and southern observations are combined. Figure 4a clearly shows that most of the enhanced flux tubes are detected within 10° latitude, while the depressed flux tubes are distributed in a much wider latitudinal region. The daily rate is defined as the counts normalized by the accumulated observation time. In the same *L* shell, for the enhanced flux tubes (Figure 4b), the daily rate is highest near the equator, while for the depressed flux tubes, the daily rate peaks from 10° to 30° latitude. This result confirms the latitudinal dependence reported in *Andre et al.* [2007] and supports the idea illustrated in Figure 1.

In Figure 4, as *L* decreases, the daily rate of both types of flux tubes first increases, reaches maximum between 6 and 10 in *L*, and then decreases. No flux tubes are detected inside $L = 4$. We suggest that as the flux tubes convect in, they break into smaller ones and, meanwhile, reload the cold plasma from the Enceladus torus. The breakup process will increase the daily rate, while the mass-loading process decreases the plasma pressure difference across the boundaries of the flux tubes and makes the magnetic signatures hard to identify. These two processes with opposite effects on the daily rate compete and result in the peak in daily rate detected at *L* from 6 to 10.

Since the plasma density in the plasma disk is a function of the radial distance, such dependence should influence the degree of compression/expansion of the flux tubes. That degree can be qualified by the magnetic pressure difference across the edges of the flux tubes. Figure 5 shows those differences as a function of *L*. It is clear that the magnitude of pressure difference across the flux tubes increases as the *L* decreases. Our interpretation of this tendency is that when the flux tubes get closer to the mass-loading region ($L \approx 4$), the increase of background cold plasma density is much faster than the refill process of the flux tubes. Therefore, the flux tubes in the plasma torus are more compressed, and more hot plasma inside the flux tube is squeezed to high latitude. In this way, for both enhanced and depressed flux tubes, the magnetic pressure difference across the boundaries increases as the *L* decreases.

Figure 5 also shows that the pressure differences associated with the depressed flux tubes are always less than those associated with the enhanced ones, indicating that the plasma pressure inside the depressed flux tubes is close to the background lobe plasma pressure.

The four different types of flux tubes, as mentioned in Figure 2, are interpreted as flux tubes detected at different ages. As *Hill et al.* [2005] discovered, the drift of energetic particles elongates the flux tubes in the azimuthal

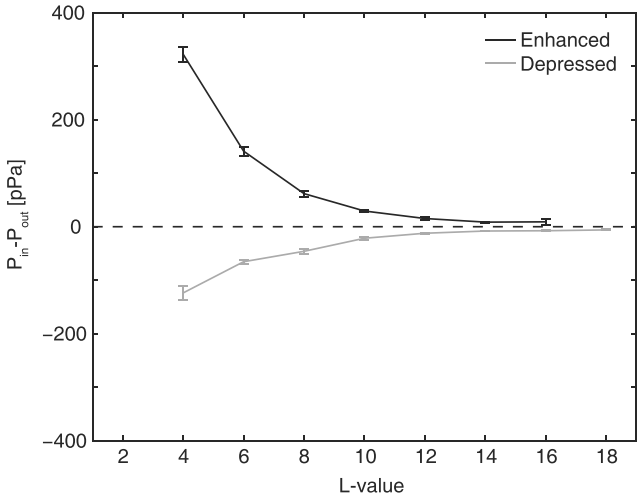

Figure 5. Magnetic pressure difference across the boundaries of the flux tubes as a function of *L*. Here the magnetic field data are classified into three independent groups by successive revolutions. The mean of the three medians calculated from each group is plotted, and the probable error is defined as the standard division divided by the square root of 2. When the observations are absent in a certain region, no error is estimated. Here the bin size is 4 and overlapped by 2 in *L*.

direction and eventually may break them up. Therefore, we suggested that type 1 and type 2 events represent the younger ones, while type 3 and type 4 events are the old ones. The relative occurrence rate of these four types of flux tubes as a function of *L* is shown in Figure 6. Here only enhanced flux tubes are counted since they are much easier to identify. It shows that type 1 and type 2 events are relatively less often detected as *L* decreases. This confirms our hypothesis that the flux tubes break into smaller ones as they convect in, similar to the case at Jupiter [*Russell et al*., 2001]. In addition, Figure 6 shows that the occurrence rate of type 1 and type 2 flux tubes are always higher than that of type 3 and type 4 events, even in small *L* regions. There are several possible reasons: (a) the flux tubes spend a longer time in type 1 and type 2 phases then quickly go through type 3 and type 4 phases, (b) the old flux tubes are always hard to identify from the background and are undercounted, and (c) there are some fast flux tubes which can reach the inner magnetosphere without significant drift taking place in the hot plasma.

4. The Origin and Transport of the Magnetic Flux

The finger or bubble cross sections of the flux tubes can be distinguished from the magnetometer data statistically, by comparing the entrance and exit normal vectors of the flux tubes. Both vectors are defined as pointing out from the flux tube. As Figure 7 illustrates, if the flux tube is circular, the angle between the two normal directions would vary from 0 to 180°, while 0° (180°) corresponds to the Cassini crossing at the edge (center). If the cross section of the flux tube is fingerlike and rooted in the plasma disk, since the radial injection velocity is much smaller than the subcorotating velocity [*Chen*, 2011], Cassini would always cross the shorter side. Therefore, the angle between the two normal directions should always be close to 180°.

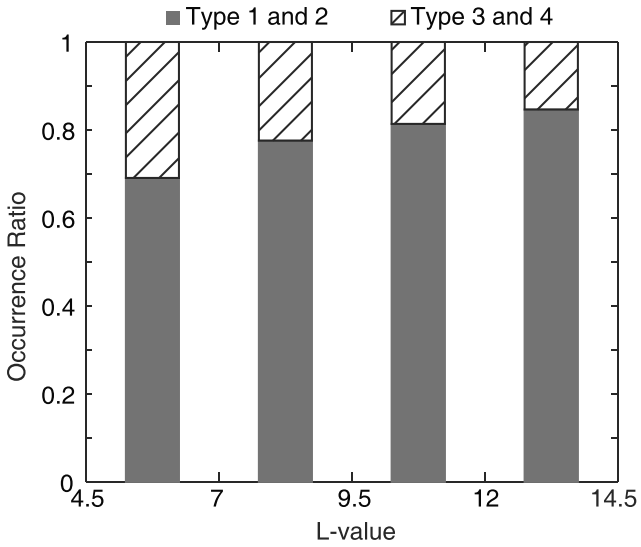

Figure 6. Occurrence ratio of different types of enhanced flux tubes.

An analysis has been presented by *Loftus et al*. [2015] using minimum variance analysis (MVA) to calculate the two normal directions. It was found that the cross sections of the flux tubes are more consistent with the circular cases. Here we use another way to determine normal vectors. Instead of MVA technique, we calculate the normal directions using $\pm \frac{\vec{B_1} \times \vec{B_2}}{\left|\vec{B_1} \times \vec{B_2}\right|}$, based on the fact that the flux tube boundaries are tangential discontinuities, while the MVA method does not guarantee zero

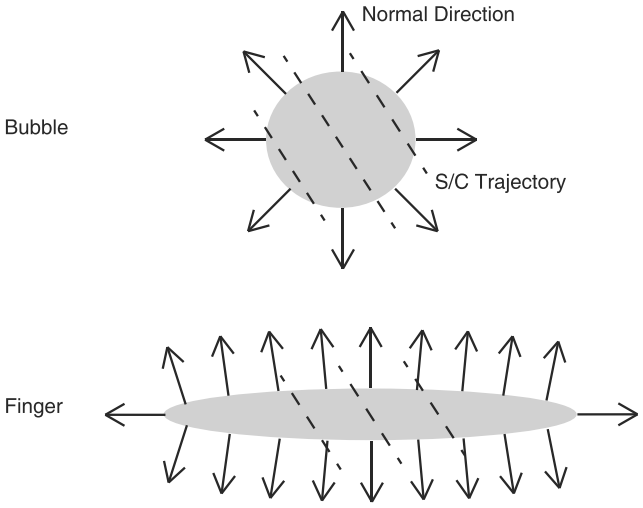

Figure 7. A cartoon illustrating the angle between the entrance and exit normal directions of the flux tubes if they are circular (up) or fingerlike (down).

normal magnetic field. Here $\vec{B_1}$ and $\vec{B_2}$ are the averaged magnetic field inside and outside the flux tube at the boundary. The plus or minus sign is chosen so that the entrance normal has a positive ϕ component, while the exit normal has a negative ϕ component in the KRTP coordinate system. In addition, if the angle between $\vec{B_1}$ and $\vec{B_2}$ at either boundary is less than 0.3°, that flux tube is not counted here.

The distribution of the angle between two normal directions is shown in Figure 8. Here only type 1 and type 2 flux tubes are studied, as their boundaries are sharp and clear. Those flux tubes are classified into two groups by L value. It is clear that over 75% flux tubes are detected with the angle being less than 160°. This distribution is against the fingerlike flux tube but favors the circular model. In addition, there is no significant difference between the distributions obtained inside and outside $L = 8.6$. This cannot be explained by the combination hypothesis [*Thomsen et al.*, 2015], which sets ~8.6 as the boundary separating reconnection and interchange processes.

In Figure 8, the number of flux tubes with the angle being larger than 90° is 5.5 times the number of flux tubes with the angle being less than 90°. This ratio is $\frac{\sqrt{2}}{2-\sqrt{2}} \approx 2.4$ if Cassini crosses flux tubes with rigidly circular cross sections randomly. The difference may be due to the undercounting of the small-angle flux tubes. Since Cassini skimmed through the flank of the flux tubes, they appear to have short durations and are hard to identify.

Since reconnection takes place in the outer magnetosphere and is beyond our observation region, it is impossible to trace the flux tube formation process with this method. However, we can use the reconnection rate to derive the transportation rate of the magnetic flux and cold plasma. If tail reconnection is the dominant mechanism in generating the inward convecting magnetic flux, the reconnection rate should be equal to the magnetic flux transportation rate. Then we can estimate the plasma transport rate: $\frac{\frac{dM}{dt}}{\rho \cdot 2 \ R_S} = \frac{\frac{d\Phi}{dt}}{B_0}$. Here $\frac{dM}{dt}$ is the mass loss rate, $\frac{d\Phi}{dt}$ is the magnetic flux transport rate, ρ is the mass density [*Holmberg et al.*, 2012], 2 R_S is the thickness of the plasma disk, and B_0 is the averaged background magnetic field strength. We use 100 kV as the reconnection rate [*Badman et al.*, 2014], and the calculated mass loss rate is listed in Table 1. We can see that from $L = 5$ to 10, this rate is almost constant at around 130 kg/s, which agrees with the plasma production rate [*Bagenal and Delamere*, 2011, and references there in]. This consistency further supports the tail reconnection mechanism.

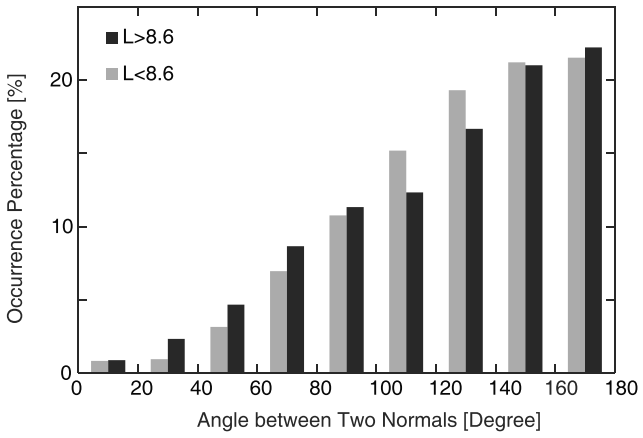

Figure 8. The distribution of the angle between the entrance and exit normal of the flux tubes.

Since the reconnection rate is the magnetic flux transportation rate, we can also estimate the inward and outward convecting velocities of both plasma and magnetic flux. The outward velocity satisfies this equation: $\frac{d\Phi}{dt} = 2\pi L R_S \left(\frac{T_{tot} - T_E}{T_{tot}}\right) V_{out} B_0$. Here T_{tot} is the total observation

Table 1. Lists of Background Magnetic Field Strength (B_0), Averaged Field Strength Inside the Flux Tube (B_E), Mass Loss Rate ($\frac{dM}{dt}$), Sum of Event Time Normalized by Total Observation Time ($\frac{T_E}{T_{tot}}$), Inflow Velocity (V_{in}), and Outflow Velocity (V_{out}) as a Function of L Value

L Value	B_0 (nT)	B_E (nT)	dM/dt (kg/s)	T_E/T_{tot} (%)	V_{in} (km/s)	V_{out} (km/s)
5–6	115.3	117.1	141.8	0.51	80.5	0.4
6–7	67.2	68.3	132.7	0.85	69.9	0.6
7–8	37.2	39.2	142.6	1.82	49.5	1.0
8–9	23.7	25.1	142.1	2.29	54.1	1.3
9–10	17.7	19.3	127.0	0.74	194.6	1.6

time and T_E is the sum of the event time. The inward velocity can be calculated by balancing the inward and outward magnetic flux flows: $V_{in}B_ET_E = V_{out}B_0(T_{tot} - T_E)$. The results are also listed in Table 1. We can see that the outward velocity is from 0.4 to 1.6 km/s, while the inward velocity is from tens to hundreds of km/s. The magnitude of the outflow velocity is consistent with the observation: ~ 0.5 km/s at $L = 5$ and generally increases to ~ 2 km/s at $L = 8.5$ [*Wilson et al.*, 2008, Figure 10]. The velocity measurements outside $L = 8.5$ scatter a lot and are not used to make comparisons here. Since our observed $\frac{T_E}{T_{tot}}$ is on average 5.6 times smaller than the one given by *Chen* [2011], the inferred inflow velocity is then 5.6 times larger than Chen's estimation. The difference in time ratio comes from different event selection criteria and different data bases. *Chen* [2011] uses plasma data to identify the injection events, which are mainly depressed flux tubes off the equator [*Chen and Hill*, 2008] and have generally longer durations (Figure 2). Here since Cassini spent most of the time near the equator, we only count the observation time and events within 10° latitude to get $\frac{T_E}{T_{tot}}$. Therefore, the enhanced flux tubes contribute most to T_E. In addition, the *Chen* [2011] data set covers 2004 to 2006, while our data set covers almost 10 years of Cassini data. Although our event time is much less than the number in *Chen* [2011], it is comparable to the number obtained at Jovian magnetosphere [*Russell et al.*, 2000]. It is noticed that the inflow velocity does not increase monotonically with increased radial distance. This is because V_{in} is very sensitive to T_E/T_{tot}, and we might have undercounted the flux tubes in the small L region. Therefore, the inflow velocity here might have been overestimated.

5. Summary

We have studied both enhanced and depressed flux tubes, which contain the returning magnetic flux from the outer magnetosphere, using almost 10 years of Cassini magnetic field data. Their detection rate, compression/expansion extent, and the temporal variation as a function of L value are investigated. The cross section of the flux tubes is found to be more circular than the fingerlike structure, which is given by simulations based on the interchange mechanism. None of those properties show any sudden change at $L \sim 8.6$, where a boundary separating the interchange-dominant inner region from the reconnection-dominant outer region had been suggested [*Thomsen et al.*, 2015]. If we match the magnetic flux transport rate with the reconnection rate, the estimated plasma loss rate and the outflow velocity are consistent with earlier observations. Therefore, reconnection is the mechanism shedding the cold plasma sourced by Enceladus and generating the returning magnetic flux.

Acknowledgments
The event lists of flux tubes are included as two tables in the supporting information S1 file.

References

Andre, N., M. K. Dougherty, C. T. Russell, J. S. Leisner, and K. K. Khurana (2005), Dynamics of the Saturnian inner magnetosphere: First inferences from the Cassini magnetometers about small-scale plasma transport in the magnetosphere, *Geophys. Res. Lett.*, *32*, L14S06, doi:10.1029/2005GL022643.

Andre, N., et al. (2007), Magnetic signatures of plasma-depleted flux tubes in the Saturnian inner magnetosphere, *Geophys. Res. Lett.*, *34*, L14108, doi:10.1029/2007GL030374.

Badman, S. V., C. M. Jackman, J. D. Nichols, J. T. Clarke, and J.-C. Gérard (2014), Open flux in Saturn's magnetosphere, *Icarus*, *231*, 137–145, doi:10.1016/j.icarus.2013.12.004.

Bagenal, F., and P. A. Delamere (2011), Flow of mass and energy in the magnetospheres of Jupiter and Saturn, *J. Geophys. Res.*, *116*, A05209, doi:10.1029/2010JA016294.

Chen, Y. (2011), Centrifugally driven radial convection of plasma in Saturn's inner magnetosphere, PhD thesis, Rice Univ., Tex.

Chen, Y., and T. W. Hill (2008), Statistical analysis of injection/dispersion events in Saturn's inner magnetosphere, *J. Geophys. Res.*, *113*, A07215, doi:10.1029/2008JA013166.

Dougherty, M. K., et al. (2004), The Cassini magnetic field investigation, *Space Sci. Rev.*, *114*, 331–383.

Hill, T. W., A. M. Rymer, J. L. Burch, F. J. Crary, D. T. Young, M. F. Thomsen, D. Delapp, N. André, A. J. Coates, and G. R. Lewis (2005), Evidence for rotationally driven plasma transport in Saturn's magnetosphere, *Geophys. Res. Lett.*, *32*, L14S10, doi:10.1029/2005GL022620.

Holmberg, M. K. G., J.-E. Wahlund, M. W. Morooka, and A. M. Persoon (2012), Ion densities and velocities in the inner plasma torus of Saturn, *Planet. Space Sci.*, *73*, 151–160.

Loftus, K., J. Vandegriff, A. Rymer, and D. Mitchell (2015), Investigating fresh hot plasma injection events in Saturn's inner magnetosphere, Abstract SM31C-2524 presented at 2015 AGU Fall Meeting, San Francisco, Calif.

Russell, C. T., M. G. Kivelson, W. S. Kurth, and D. A. Gurnett (2000), Implications of depleted flux tubes in the Jovian magnetosphere, *Geophys. Res. Lett.*, *27*, 3133–3136, doi:10.1029/2000GL003815.

Russell, C. T., M. G. Kivelson, W. S. Kurth, and D. A. Gurnett (2001), Depleted magnetic flux tubes as probes of the Io torus plasma, *Adv. Space Res.*, *28*(10), 1489–1493.

Siscoe, G. L., and D. Summers (1981), Centrifugally driven diffusion of logenic plasma, *J. Geophys. Res.*, *86*, 8471–8479, doi:10.1029/JA086iA10p08471.

Thomsen, M. F., D. G. Mitchell, X. Jia, C. M. Jackman, G. Hospodarsky, and A. J. Coates (2015), Plasmapause formation at Saturn, *J. Geophys. Res. Space Physics*, *120*, 2571–2583, doi:10.1002/2015JA021008.

Vasyliunas, V. M. (1983), Plasma distribution and flow, in *Physics of the Jovian Magnetosphere*, edited by A. J. Dessler, pp. 395–453, Cambridge Univ. Press, New York.

Wilson, R. J., R. L. Tokar, M. G. Henderson, T. W. Hill, M. F. Thomsen, and D. H. Pontius Jr. (2008), Cassini plasma spectrometer thermal ion measurements in Saturn's inner magnetosphere, *J. Geophys. Res.*, *113*, A12218, doi:10.1029/2008JA013486.

Winglee, R. M., A. Kidder, E. Harnett, N. Ifland, C. Paty, and D. Snowden (2013), Generation of periodic signatures at Saturn through Titan's interaction with the centrifugal interchange instability, *J. Geophys. Res. Space Physics*, *118*, 4253–4269, doi:10.1002/jgra.50397.

Wu, H. (2009), Rice convection model simulations of the centrifugal interchange instability in the magnetospheres of Jupiter and Saturn, PhD thesis, Rice Univ., Tex.